PASJ: Publ. Astron. Soc. Japan **59**, 547–558, 2007 June 25

Stellar Contents of Two Intermediate Age Clusters: NGC 1912 and NGC 1907

Anil K. PANDEY,[1,2] Saurabh SHARMA,[1] Karunakar UPADHYAY,[1] Katsuo OGURA,[3] Tejbir S. SANDHU,[1] Hiroyuki MITO,[4] and Ram SAGAR[1]

[1]*Aryabhatta Research Institute of Observational Sciences, Manora Peak, Nainital 263 129, Uttaranchal, India*

[2]*Institute of Astronomy, National Central University, Chung-Li 32054, Taiwan*

pandey@aries.ernet.in

[3]*Kokugakuin University, Higashi, Shibuya-ku, Tokyo 150-8440*

[4]*Kiso Observatory, School of Science, The University of Tokyo, Mitake-mura, Kiso-gun, Nagano 397-0101*

(Received 2006 November 10; accepted 2007 February 13)

Abstract

We present CCD photometry in a wide field around two open clusters, NGC 1912 and NGC 1907. The stellar surface density profiles indicate that the radii of the clusters NGC 1912 and NGC 1907 are $\sim 14'$ and $\sim 6'$ respectively. The core of the cluster NGC 1907 is found to be $1'.6 \pm 0'.3$, whereas the core of the cluster NGC 1912 could not be defined due to its significant variation with the limiting magnitude. The clusters are situated at distances of 1400 ± 100 pc (NGC 1912) and 1760 ± 100 pc (NGC 1907), indicating that in spite of their close locations on the sky they may be formed in different parts of the Galaxy. Although the mass functions for the clusters are quite noisy, in the given mass range the slopes of the mass functions for clusters NGC 1912 and NGC 1907 turn out to be -1.12 ± 0.30 and -1.23 ± 0.21, respectively, which are in agreement with the Salpeter value. Because the ages of the clusters are much higher than the estimated relaxation time-scales, dynamical relaxation may be one of the reasons for the observed mass segregation in the clusters. A comparison of the observed CMDs of the clusters with the synthetic CMDs gives a photometric binary content as $30 \pm 10\%$ (mass range $1.0 \leq M_{\odot} \leq 3.1$) and $20 \pm 10\%$ (mass range $1.2 \leq M_{\odot} \leq 3.2$) in the case of NGC 1912 and NGC 1907, respectively.

Key words: binaries: general — open clusters and associations: individual (NGC 1912, NGC 1907) — stars: HR and C–M diagrams — stars: luminosity function, mass function — techniques: photometric

1. Introduction

The stability of an open cluster in the Galaxy depends upon its structure. Kholopov (1969) found that the nucleus and the corona (the extended region of the cluster) are two main regions in open clusters. Because the nucleus of the clusters contains relatively bright and massive stars, it is a well-studied region of the clusters. However, the corona of star clusters, which generally contains a large number of faint stars, has not been studied in detail. In fact, the spatial distribution of these faint and low-mass stars ($M \leq 1 M_{\odot}$) defines the actual boundary of the cluster. Consequently, coronal regions have important bearing on studies related to the mass function (MF), the structure and the evolution of open clusters.

Extensive studies of the coronal regions of open clusters have not been carried out so far mainly because of the non-availability of photometry in a large field around open star clusters. We have undertaken a CCD photometric study of a large area around open clusters using the 2 K × 2 K CCD mounted on the 105 cm Schmidt telescope of the Kiso Observatory, which gives an $\sim 50' \times 50'$ field, and the 2 K × 2 K CCD mounted on the 104 cm Sampurnanand telescope of Aryabhatta Research Institute of Observational Sciences (ARIES), Nainital (cf. Pandey et al. 2001, 2005). In this paper we report on an analysis of CCD photometric observations of NGC 1912 and NGC 1907.

The open clusters NGC 1907 [RA (J2000.0) = $05^{\rm h}28^{\rm m}05^{\rm s}$, Dec (J2000.0) = $35°19'30''$] and NGC 1912 [RA (J2000.0) = $05^{\rm h}28^{\rm m}40$, Dec (J2000.0) = $35°50'54''$] are situated in the anti-center direction of the Galaxy in the constellation of Auriga. Figures 1 and 2 show V-band image of clusters NGC 1912 and NGC 1907, respectively.

Johnson (1961) estimated the distance and the reddening $E(B-V)$ of NGC 1912 to be 1320 pc and 0.27 mag respectively, while the corresponding values reported by Becker (1963) are 1415 pc and 0.24 mag, respectively. Using photoelectric photometry, Hoag and Applequist (1965) reported a distance of ~ 870 pc and $E(B-V) = 0.27$ mag. Kharchenko et al. (2005) have reported a distance of 1066 pc, $E(B-V) = 0.25$ mag and log age = 8.56 for the cluster. Subramaniam and Sagar (1999, hereafter SS99) carried out CCD photometry for the cluster in a $7' \times 14'$ field, and found distance, reddening $E(B-V)$ and age values of 1820 pc, 0.23 mag and 250 Myr, respectively. Recently Jacobson et al. (2002) reported a UBV CCD photometry in a field of $\sim 20' \times 20'$, and found distance modulus, reddening and age values of 10.71, 0.24 mag and 375 Myr, respectively.

On the sky NGC 1907 is located close to NGC 1912. The distance to the cluster is reported to be 2750 pc, 4750 pc, and 1380 pc by Trumpler (1930), Collinder (1931), and Becker (1963), respectively. Hoag (1966) found a distance of 1380 pc and reddening $E(B-V) \sim 0.38$ mag, whereas Purgathofer (1961) reported the distance and reddening for NGC 1907 to be 1380 pc and 0.47 mag, respectively. CCD photometry

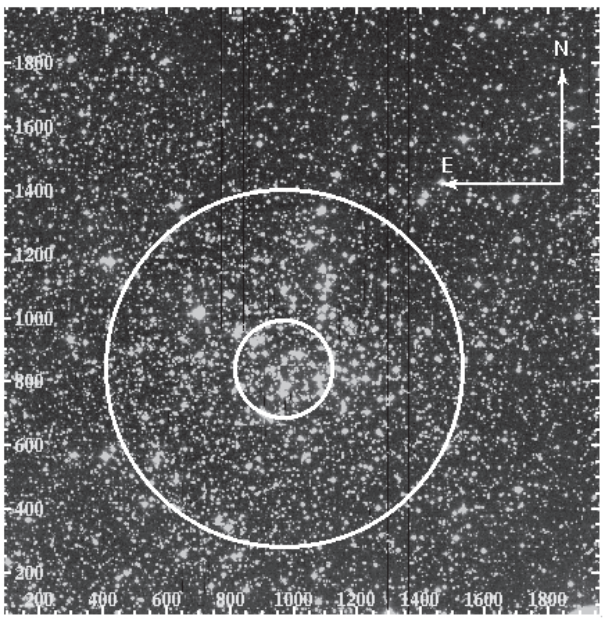

Fig. 1. V band image of the cluster NGC 1912. The circles show the core and boundary of the cluster obtained in the present work.

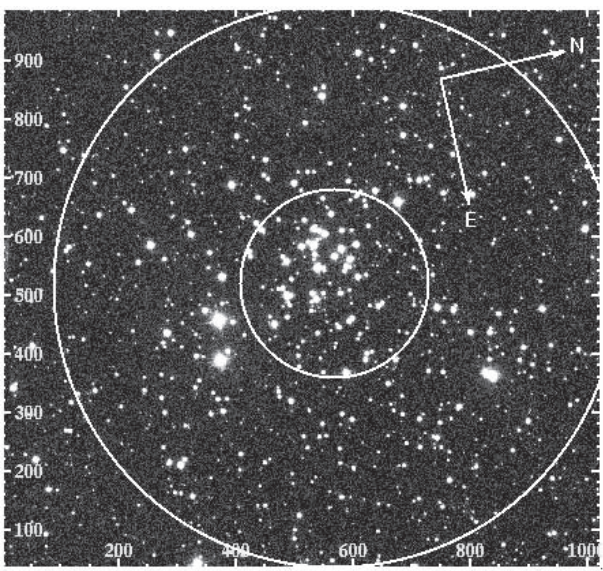

Fig. 2. Same as figure 1 but for the cluster NGC 1907.

in a $2'.28 \times 3'.43$ field by SS99 yields distance, reddening $E(B-V)$, and age values of 1785 pc, 0.40 ± 0.05 mag, and 400 Myr, respectively. Recently, Kharchenko et al. (2005) reported a distance of 1556 pc, $E(B-V) = 0.42$ mag, and log age $= 8.57$ for the cluster.

SS99 suggested that the clusters NGC 1912 and NGC 1907 are candidates for a physical pair. The photometry of SS99 shows rather high photometric errors, as can be seen from the errors reported in their table 3. For the $V = 17$–18 mag range they report errors in B, V, R, I passbands of 0.070, 0.095, 0.063, and 0.11, respectively. Therefore, it is felt worthwhile to procure new data for these two clusters. The accuracy of the present CCD photometric observations is much better than that reported by SS99. In a recent study, de Oliveira et al. (2002) concluded that these clusters were formed in different parts of the Galaxy. They also suggested that it is necessary to analyze deep wide field CCD photometry for a more conclusive result about the apparent absence of a tidal link between these clusters.

As we mentioned earlier, the aim of the Kiso project is to provide homogeneous data of open clusters towards the anti-center direction of the Galaxy; the data of these clusters will provide useful input to study the structure of the Norma–Cygnus (outer) spiral arm, which is discussed in detail in another paper (Pandey et al. 2006). The aim of the present paper is to analyze a deep and wide field around NGC 1907 and NGC 1912 to study the structure, MF, mass segregation effect, and stellar evolutionary aspects of the clusters. Observations and comparisons with the previous photometries are given in the next section. The cluster radius, other photometric results, and MF of the cluster are described in subsequent sections.

2. Observations and Data Reduction

2.1. NGC 1912

CCD $BVI_{\rm c}$ observations of the cluster NGC 1912 were obtained using the 105 cm Schmidt telescope of the Kiso Observatory on 1999 November 3. The CCD camera used a SITe 2048 × 2048 TK2048E chip having a pixel size of 24 μm. At the Schmidt focus ($f/3.1$) each pixel corresponds to $1''.5$, and the entire chip covers a field of $\sim 50' \times 50'$ on the sky. The read-out noise and the gain of the CCD are 23.2 e^- and 3.4 e^-/ADU, respectively. The FWHM of the star images was $\sim 4''$. A number of bias and dome flat frames were also taken during the observing runs.

2.2. NGC 1907

The CCD $BV(RI)_{\rm c}$ data were acquired on 2004 December 18 using the 2048×2048 pixel CCD camera mounted on the $f/13$ Cassegrain focus of the 104 cm Sampurnanand telescope of ARIES, Nainital. In this set-up, each pixel of the CCD corresponds to $0''.37$, and the entire chip covers a field of $\sim 13' \times 13'$ on the sky. To improve the signal-to-noise ratio, the observations were carried out in a binning mode of 2×2 pixels. The FWHM of the star images was $\sim 2''$.

2.3. Blank Field

We also observed a field of $\sim 13' \times 13'$ located at a distance of $\sim 45'$ away towards east of the cluster center, NGC 1912, using the 104 cm Sampurnanand telescope. The statistics of the field region was used to remove field star contamination, while estimating the luminosity function (LF) and MF.

The log of observations is given in table 1. The observations were standardized by observing standard stars in SA 98 (Landolt 1992) on two nights using a 2048×2048 pixel CCD camera (for NGC 1912 and blank field) and a 1024×1024 pixel CCD camera (for NGC 1907) mounted on the 104 cm Sampurnanand telescope of ARIES. Short exposures of both cluster regions and a blank-field region were taken on the standardization night.

A data analysis was carried out at ARIES, Nainital using the ESO MIDAS and DAOPHOT II software packages. The

point-spread function (PSF) was obtained for each frame using several uncontaminated stars. The image parameters and errors provided by DAOPHOT were used to reject poor measurements (cf. Pandey et al. 2001). Calibration of the instrumental magnitude to the standard system was done using a procedure outlined by Stetson (1992). The photometric calibration equations used were as follows:

$$b = B + c_2 + m_2(B-V) + k_b X, \quad (1)$$

$$v = V + c_3 + m_3(V-I) + k_v X, \quad (2)$$

$$r = R + c_4 + m_4(V-R) + k_r X, \quad (3)$$

$$i = I + c_5 + m_5(V-I) + k_i X, \quad (4)$$

where B, V, R, and I are the standard magnitudes; b, v, r, and i are the instrumental magnitudes normalized for 1 second of exposure time and X is the air mass; c_2, c_3, c_4, c_5, and m_2, m_3, m_4, m_5 are zero-point constants and colour-coefficients respectively; and k_b, k_v, k_r, k_i are extinction coefficients in B, V, R, and I bands, respectively. The values of the zero-point constants, colour coefficients, and extinction coefficients in various bands are given in table 2.

Figure 3 shows the standardization residual, Δ, between the standard and transformed V magnitude and $(B-V), (V-R)$, and $(V-I)$ colours of standard stars. The standard deviations in ΔV, $\Delta(B-V)$, $\Delta(V-R)$, and $\Delta(V-I)$ are 0.004, 0.007, 0.012, and 0.006 mag, respectively, in the case of NGC 1907 and 0.024, 0.028, and 0.020 in the case of NGC 1912 and the blank field region. Short exposures of cluster regions and the blank region, taken on two standardization nights, were standardized using the above equations and coefficients. The standard magnitude and colours of more than 50 stars obtained from these short exposures were further used to standardize the deep observations taken on 1999 November 3, 2001 October 15, and 2004 December 18. The standard deviations of the residual of secondary standards are on the order ~ 0.01 mag.

The photometric data along with the positions of stars measured in the clusters are given in tables 3 and 4 for clusters NGC 1912 and NGC 1907, respectively. These tables are available in the electronic form only. The format of tables 3 and 4 is shown here. The larger value of the mean errors at each magnitude bin, given by DAOPHOT and ADDSTAR routine (cf. section 6), is adopted as the mean errors; these are given in table 5.

Table 1. Log of observations.

Cluster (date)	Filter	Exposure (s) × number of frames
NGC 1912 (1999 11 03)	B	$60\times3, 20\times9$
	V	$60\times3, 10\times9$
	I	$60\times3, 10\times11$
NGC 1907 (2004 12 18)	B	$600\times3, 30\times4$
	V	$600\times3, 30\times4$
	R	$300\times4, 30\times3, 10\times3$
	I	$300\times4, 30\times3, 10\times3$
Blank field (2001 10 15)	V	600×4
	I	300×4

3. Comparison with Previous Photometries

A comparison of the present CCD photometry with the available photoelectric photometry and CCD photometry has been carried out. The difference Δ (present data − literature) as a function of the V magnitude is shown in figures 4 and 5, and statistical results are given in table 6. In the case of NGC 1912, the comparison indicates that the colours and the magnitude obtained in the present work are in fair agreement with those reported by Hoag et al. (1961). A comparison with the CCD photometry of SS99 indicates a significantly large scatter. The V magnitudes by SS99 show a trend, and become brighter with increasing V magnitude.

In the case of NGC 1907, the comparison indicates the following:

(i) The colour and magnitude obtained by us are in agreement with those given by Purgathofer (1964). The comparison with the data by Hoag et al. (1961) indicates that the present V magnitudes are in agreement with their estimation, whereas the present $(B-V)$ colours are bluer by ~ 0.04 mag.

(ii) The V magnitudes reported by SS99 (CCD) are systematically bright by ~ 0.1 mag compared with those reported in the present study. The comparison of the $(B-V)$ colour in the case of NGC 1907 also indicates a large scatter and the $(B-V)$ colour by SS 99 becomes blue compared with the present colours by ~ 0.1 mag at $V = 17$–18 mag.

Table 2. The zero-point constants, color coefficients and extinction coefficients.

Object	Zero-point constant	Colour coefficient	Extinction coefficient
NGC 1907:			
	$c_2 = 6.022 \pm 0.005$	$m_2 = -0.143 \pm 0.004$	$k_b = 0.37 \pm 0.01$
	$c_3 = 5.294 \pm 0.004$	$m_3 = \ \ 0.002 \pm 0.003$	$k_v = 0.28 \pm 0.01$
	$c_4 = 4.794 \pm 0.004$	$m_4 = \ \ 0.062 \pm 0.006$	$k_r = 0.22 \pm 0.01$
	$c_5 = 4.947 \pm 0.005$	$m_5 = -0.038 \pm 0.004$	$k_i = 0.16 \pm 0.01$
NGC 1912 and blank field:			
	$c_2 = 4.678 \pm 0.030$	$m_2 = -0.056 \pm 0.019$	$k_b = 0.23 \pm 0.01$
	$c_3 = 4.254 \pm 0.024$	$m_3 = -0.038 \pm 0.018$	$k_v = 0.15 \pm 0.01$
	$c_5 = 4.699 \pm 0.024$	$m_5 = -0.068 \pm 0.018$	$k_i = 0.06 \pm 0.01$

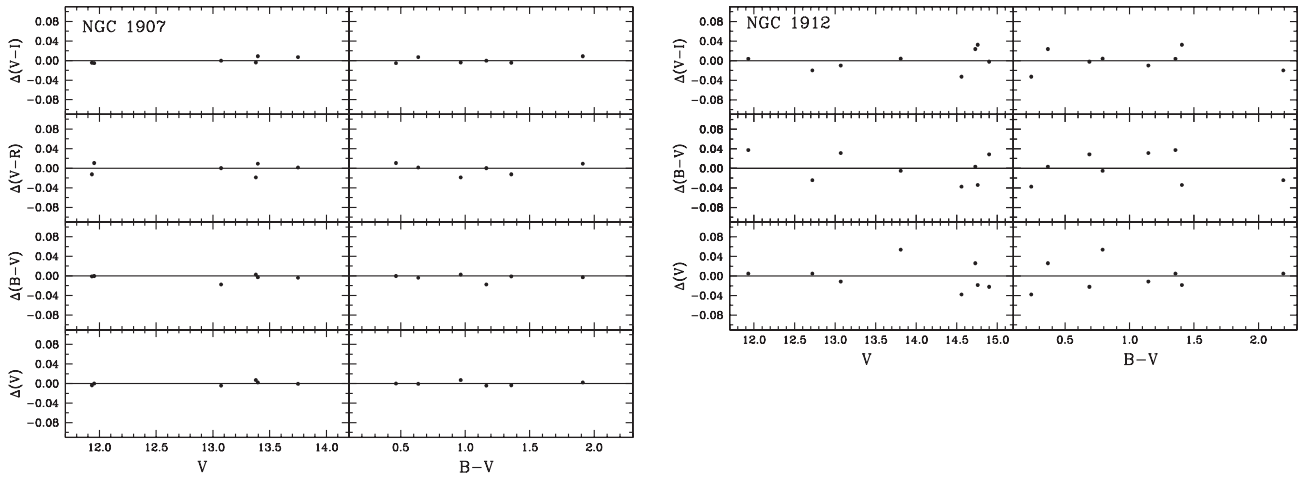

Fig. 3. Residuals between standard and transformed magnitudes and colours of standard stars plotted against standard V magnitude and $(B-V)$ colour.

Table 3. BVI_c photometric data of the stars in the field of NGC 1912.*

Sequence	X (pixel)	Y (pixel)	V (mag)	$B-V$ (mag)	$V-I$ (mag)	Radius (arcsec)
1	978.15	843.52	20.183	–	1.650	19.74
2	961.98	857.74	15.126	0.507	0.616	21.10
3	948.83	847.12	13.507	0.376	0.507	24.70
4	981.14	838.74	17.371	0.845	0.948	25.46

* X, Y are the pixel coordinates. The radius is with respect to the center $X = 965$, $Y = 844$. All contents of the table can be found in the electronic version.[1]

Table 4. Photometric data of the stars in the field of NGC 1907.*

Sequence	X (pixel)	Y (pixel)	V (mag)	$B-V$ (mag)	$V-I$ (mag)	$V-R$ (mag)	Radius (arcsec)
1	559.27	521.94	16.452	0.935	1.100	0.552	4.89
2	572.60	523.72	19.541	1.617	1.703	0.905	5.14
3	576.03	513.67	18.255	1.184	1.181	0.544	8.94
4	548.06	522.08	20.784	1.270	1.510	0.773	12.94

* X, Y are the pixel coordinates. The radius is with respect to the center $X = 566$, $Y = 521$. All contents of the table can be found in the electronic version.[1]

The right-hand panels of figures 4 and 5 show a comparison of SS99 and the present photometry with the photoelectric photometry as a function of the $(B-V)$ colour. A comparison indicates that in the case of NGC 1912 the V magnitude and the $(B-V)$ colour obtained in the present study agree fairly well [$\Delta V = -0.01 \pm 0.05$, $\Delta(B-V) = -0.04 \pm 0.05$] with the photoelectric data by Hoag et al. (1961), whereas the data by SS99 manifest a shift in the V magnitude of ~ 0.16 mag and ~ 0.06 mag in $(B-V)$.

In the case of NGC 1907, the present V magnitude agrees fairly well with the photoelectric data, whereas the V magnitude by SS99 shows a systematic shift of ~ 0.1 mag. The comparison of colours indicates that in the $(B-V)$ range 0.2–0.4 mag, the present $(B-V)$ colours are bluer by $\sim$ 0.05 mag. However, in the $(B-V)$ range 0.4 to 0.9 mag the colours match with the photoelectric data. Since probable members of the cluster have $(B-V) \geq 0.4$ (cf. section 5), and since we have used standard stars having $0.463 \leq B-V \leq 1.909$ for the calibration purpose, we do not expect any problem in the calibration for stars having $(B-V) \geq 0.4$.

4. Radial Stellar Surface Density

Because the area of observation is sufficiently large, the present CCD observations can be used to study the radial extent and structure of the cluster. The center of the cluster was determined using the stellar density distribution of stars having $V \leq 18$ mag, in a ± 300 pixel wide strip along both the X and Y directions around the eye-estimated center. The point of maximum density obtained by fitting a Gaussian curve is considered to be the center of the cluster. The (X, Y) pixel

[1] ⟨http://pasj.asj.or.jp/v59/n3/590311/⟩.

Table 5. Average photometric errors σ's as a function of brightness.

Cluster	Magnitude range	σ_B	σ_V	σ_R	σ_I
NGC 1912	< 12	0.02	0.02		0.02
	12–13	0.02	0.03		0.03
	13–14	0.02	0.03		0.03
	14–15	0.02	0.03		0.03
	15–16	0.02	0.03		0.03
	16–17	0.03	0.03		0.03
	17–18	0.03	0.03		0.04
	18–19	0.04	0.04		0.06
	19–20	0.05	0.06		0.10
NGC 1907	< 12	0.01	0.01	0.01	0.01
	12–13	0.01	0.01	0.01	0.01
	13–14	0.01	0.01	0.01	0.01
	14–15	0.01	0.01	0.01	0.01
	15–16	0.01	0.01	0.02	0.02
	16–17	0.02	0.02	0.02	0.02
	17–18	0.02	0.02	0.03	0.03
	18–19	0.03	0.03	0.04	0.04
	19–20	0.05	0.05	0.05	0.06
	20–21	0.07	0.07	0.07	0.07
	21–22	0.08	0.08	0.08	0.08

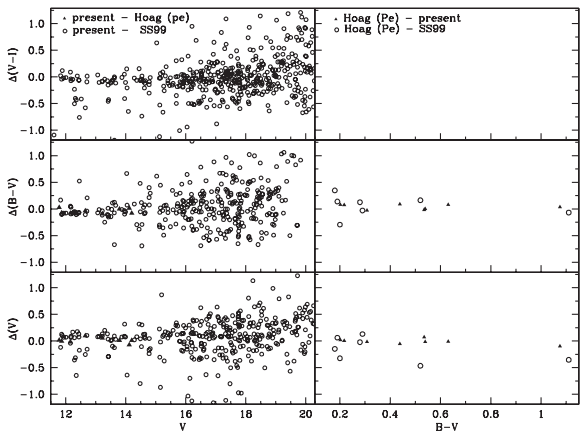

Fig. 4. Left panel: comparison of the present CCD photometry of NGC 1912 with the photoelectric photometry (filled triangle) by Hoag et al. (1961) and with the CCD photometry (open circles) by SS99 respectively. Right panel: comparison of the present and SS99 photometry with the photoelectric photometry as a function of $(B-V)$.

coordinates of the cluster centers are found to be (566, 521; NGC 1907) and (965, 844; NGC 1912), which correspond to RA(J2000.0) = $05^{\rm h}28^{\rm m}09^{\rm s}$, Dec (J2000.0) = $35°19'30''$ and RA(J2000.0) = $05^{\rm h}28^{\rm m}50^{\rm s}$, Dec (J2000.0) = $35°48'45''$ respectively.

To determine the radial surface density we divided the cluster into a number of concentric circles. The projected radial stellar density in each concentric circle was obtained by dividing the number of stars in each annulus by its area. The densities thus obtained are plotted in the upper panels of figures 6 and 7 for the clusters NGC 1912 and NGC 1907,

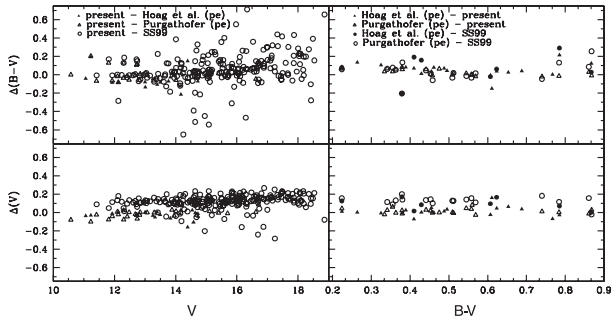

Fig. 5. Comparison of the present CCD photometry of NGC 1907 with the photoelectric photometry (filled triangles: Hoag et al. 1961; open triangles: Purgathofer 1964) and with the CCD photometry (open circles) by SS99 respectively. Right panel: comparison of present and SS99 photometry with the photoelectric photometry as function of $(B-V)$.

respectively. The error bars were derived by assuming that the number of stars in a concentric annulus follow Poisson statistics. The horizontal dashed line in the plot indicates the density of contaminating field stars, which was obtained from the frame observed at a distance of $\sim 45'$ away towards east of the NGC 1912 cluster center. The density distribution shown in the upper panels of figures 6 and 7 may be affected by the presence of field stars. Only on the basis of photometry, it is difficult to separate the cluster members from the field stars. However, the contribution of the field stars can be reduced if we select a sample of stars near a well defined main-sequence (MS) in the colour–magnitude diagram. To select such a sample we defined blue and red envelopes for the MS (cf. Pandey et al. 2001, 2005); the radial density distribution of the MS sample is also shown in the lower panels of figures 6 and 7. Both samples show almost similar radial distributions of the density. The radial distribution of stars indicates that the extents of NGC 1912 and NGC 1907 are $\sim 14'$ and $\sim 6'$, respectively. The stellar density near the boundary of both clusters matches (within 3σ error) with the stellar density obtained from the blank field.

To parametrize the radial density profiles, we follow the approach by Kaluzny and Udalski (1992). Because of the low S/N ratio in the star counts of open clusters, it is not an easy task to constrain the tidal radius of a cluster using the empirical model of King (1962). We describe the radial density, $\rho(r)$, as

$$\rho(r) = \frac{f_0}{1 + \left(\frac{r}{r_{\rm c}}\right)^2}, \qquad (5)$$

where $r_{\rm c}$ is the core radius (the radius at which the surface density falls to half of the central density, f_0). We fit the above function to the observed radial density profile of stars. The best fit was obtained by the χ^2 minimization technique.

In the case of NGC 1912, the fit was performed for data within radii of $22'$. The core radius for the radial density profile shown in the upper panel of figure 6 turns out to be $3'.8$, whereas it turns out to be $4'.5$ for MS stars (lower panel). However, the core radius for various magnitude levels ($16 \leq V \leq 19$) varies from $3'.3$ to $9'.0$. To study various parameters, e.g., colour–magnitude diagrams (CMDs), MF, etc., in detail

Table 6. Comparison of the present CCD photometry with the available photometries in the literature.*

		V-range	$\Delta(V)$ Mean$\pm\sigma$	N	$\Delta(B-V)$ Mean$\pm\sigma$	N	$\Delta(V-I)$ Mean$\pm\sigma$	N
NGC 1912	SS99 (CCD)	11–12	−0.04±0.11	4	−0.03±0.13	4	0.02±0.07	4
		12–13	−0.02±0.18	15	0.01±0.17	15	−0.18±0.26	15
		13–14	−0.03±0.15	20	−0.08±0.14	20	−0.12±0.15	20
		14–15	0.04±0.16	14	0.01±0.23	14	−0.08±0.11	14
		15–16	0.08±0.18	27	−0.07±0.18	26	−0.10±0.13	27
		16–17	0.07±0.25	54	−0.01±0.34	48	−0.06±0.25	54
		17–18	0.12±0.28	71	0.02±0.39	62	−0.03±0.30	71
		18–19	0.15±0.25	56	0.05±0.35	47	−0.02±0.33	56
		19–20	0.20±0.29	40	0.17±0.17	5	−0.04±0.34	40
	Hoag et al. (1961) (pe)	11–12	0.01±0.01	2	−0.02±0.07	2		
		12–13	0.04±0.08	2	−0.06±0.03	2		
		13–14	0.03±0.03	2	−0.05±0.06	2		
		14–15	−0.03±0.06	2	−0.03±0.07	2		
NGC 1907	SS99 (CCD)	13–14	0.11±0.05	19	−0.00±0.09	19		
		14–15	0.10±0.07	42	−0.04±0.35	42		
		15–16	0.11±0.07	47	0.02±0.28	47		
		16–17	0.13±0.09	48	−0.00±0.44	48		
		17–18	0.14±0.11	30	0.14±0.16	30		
	Purgathofer (1964) (pe)	11–12	−0.06±0.03	4	0.05±0.14	4		
		12–13	−0.02±0.03	11	0.01±0.07	11		
		13–14	−0.00±0.03	4	−0.01±0.04	4		
		14–15	−0.01±0.03	2	−0.03±0.05	2		
	Hoag et al. (1961) (pe)	11–12	−0.03±0.01	3	0.02±0.15	3		
		12–13	0.01±0.00	1	−0.08±0.00	1		
		13–14	−0.01±0.04	8	−0.07±0.04	8		
		14–15	−0.02±0.07	9	−0.03±0.10	9		

* The difference Δ (present data − literature) is in magnitude. Mean and σ are based on N in a V magnitude bin. CCD = charge-coupled devices, pe = photoelectric.

we divided the cluster into two subregions as the inner region ($r \leq 6'$), and the outer region ($6' < r \leq 14'$).

In the case of NGC 1907, the best fit of the above function to the observed radial density profile, shown in figure 7, gives a core radius values of $r_c = 1'.6 \pm 0'.3$, also, the radial extent of the cluster is estimated to be $\sim 6'$. In ensuing sections, the cluster properties are considered in detail in two sub-regions having $r \leq 2'$ (core) and $2' < r \leq 6'$ (corona).

5. Colour Magnitude Diagrams

Colour–magnitude diagrams (CMDs) for stars lying in the cluster region are shown in figures 8 and 9. The V, $(V-I)$ CMD for the nearby field region is shown in figure 10. The CMDs of the cluster regions show a well-defined, but relatively broad main sequence. The broadening of the MS may be due to:

(i) variable reddening in the cluster region,
(ii) presence of field stars in the sample,
(iii) internal error of the photometry,
(iv) presence of binaries and peculiar stars in the cluster.

Since the clusters are of intermediate age and the error in the magnitude estimation is ~ 0.04 mag for stars having $V \leq 17.0$, the first and third points may not be the main factors for broadening of the MS. However, the errors increase rapidly for stars having $V > 17.0$ and the effect of photometric errors is obvious in the CMDs. The presence of field stars and probable binaries may be the main cause for broadening of the MS. Although it is difficult to separate field stars from cluster stars, we can reduce the contamination of field stars if we restrict ourselves to the central portion of the cluster.

5.1. NGC 1912

Since most of the bright stars are saturated even on our short exposure frames, we supplemented the present CCD observations with the photoelectric photometry for bright stars by Hoag et al. (1961). A normal value for the colour-excess ratio, $E(V-R)/E(B-V) = 0.60$ and $E(V-I)/E(B-V) = 1.25$ was used for both the clusters. In figure 8 we have over-plotted the isochrones by Bertelli et al. (1994) for $Z = 0.02$ and log age = 8.5, assuming a mean reddening of $E(B-V) = 0.25$ mag, finding a mean apparent distance modulus of $(V - M_V) = 11.5$ mag, which corresponds to a distance of ~ 1400 pc. The estimated distance is in good agreement with those reported Johnson (1961; 1320 pc) and Becker (1963; 1415 pc). Recently, Jacobson et al. (2002) also reported a distance modulus of $m - M = 10.71$ mag (distance ~ 1380 pc) and a cluster age of 375 Myr. The distance

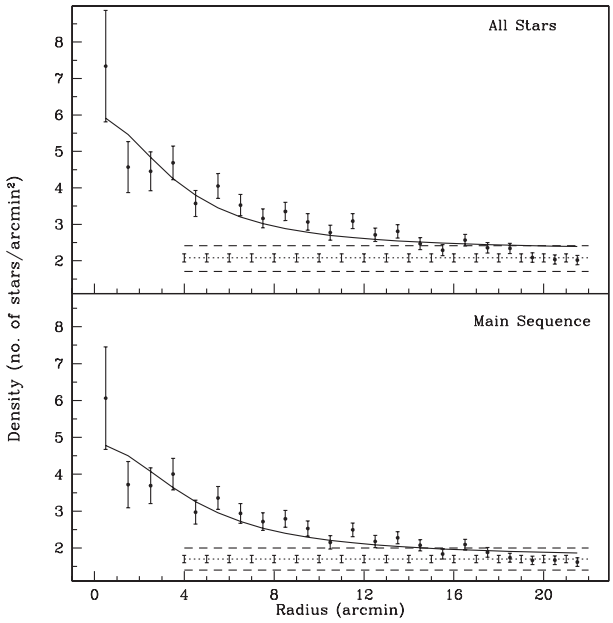

Fig. 6. Radial variation of the projected stellar density of stars (filled circles) having $V \leq 18$ in the NGC 1912 cluster region. The continuous curve represents a least-squares fit of the King (1962) profile to the observed data points (see text). The error bars represent $1/\sqrt{N}$ errors. The short dashed line indicates the density of field stars. The long dashed lines show $\pm 3\sigma$ boundaries.

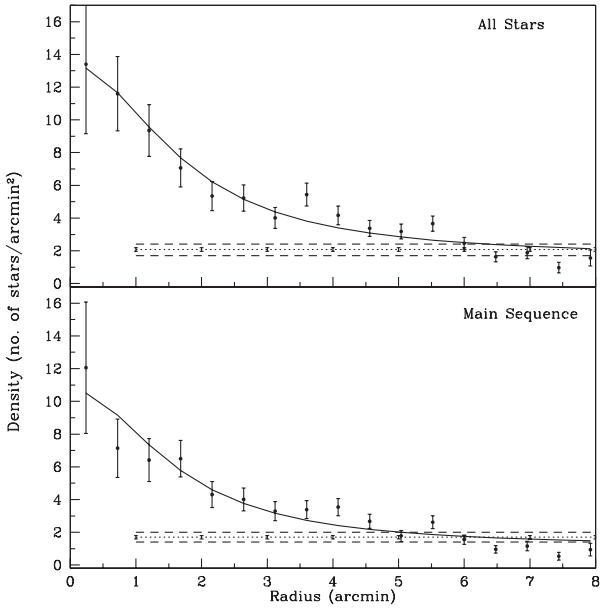

Fig. 7. Same as figure 6, but for NGC 1907.

estimated by earlier studies lies in the range of 870 pc (Hoag & Applequist, 1965)–1820 pc (SS99). Using a mean value of $E(B-V) = 0.23$ mag, SS99 obtained the distance modulus by fitting the isochrone to the blue envelope of the observed MS. The CMDs reported by SS99 show a large dispersion, and the fit to the MS blue envelope of their data may yield a large value for the distance.

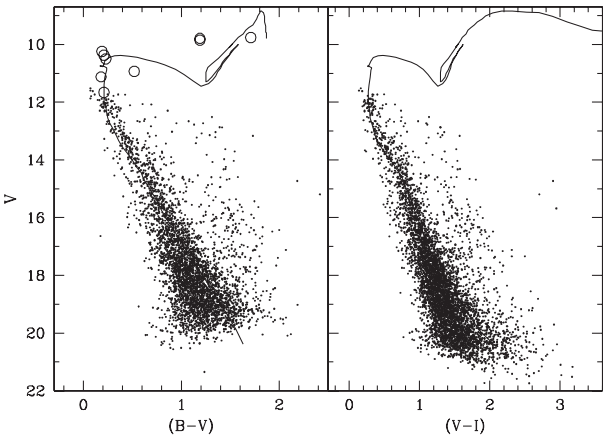

Fig. 8. CMDs for NGC 1912. The isochrones by Bertelli et al. (1994) for solar metallicity and log age = 8.5 are also shown. The open circle represents photoelectric data by Hoag et al. (1961)

5.2. NGC 1907

Adopting a mean reddening of $E(B-V) = 0.38$ mag (Hoag 1966), an isochrone of log age = 8.6 having solar metallicity by Bertelli et al. (1994) is over-plotted on the CMDs shown in figure 9, leading to a distance modulus of $(m-M) = 12.4$. The apparent distance modulus corresponds to a distance of 1760 pc. The estimates of distance to the cluster NGC 1907 reported in the literature show a large difference (1380 pc to 4750 pc). The location of evolved stars in both the clusters is nicely explained by the isochrones shown in figures 8 and 9.

Keeping in mind the errors in the reddening estimation and the distance modulus, the expected error in the distance estimation of these clusters is about 100 pc.

6. Mass Function

With the help of CMDs we could derive the observed LF of the probable MS cluster members, and then the MF using the theoretical evolutionary models of Bertelli et al. (1994). The LF, defined as the distribution of stars per unit magnitude range, can in principle be obtained from observations in one wavelength band only. However, we know that the cluster region is contaminated by the field stars, and with only a single passband we cannot decide whether the star is really a member of the cluster. Two passbands, such as V and I, are required to identify the cluster members. We used the V, $(V-I)$ CMD to determine the membership and to construct the LF of the cluster.

The photometric data may be incomplete due to various reasons, e.g., crowding of the stars. An incompleteness correction is necessary if we want to analyze the LF/MF of the stars in the cluster. To determine the completeness factor we used the ADDSTAR routine of DAOPHOT II, as described in detail in our earlier work (Pandey et al. 2001). The completeness factor, CF, is given in table 7 and it is used to correct data for incompleteness. As expected, the incompleteness of the data increases with increasing magnitudes and increasing stellar crowding.

To study the LF/MF, it is necessary to remove field star

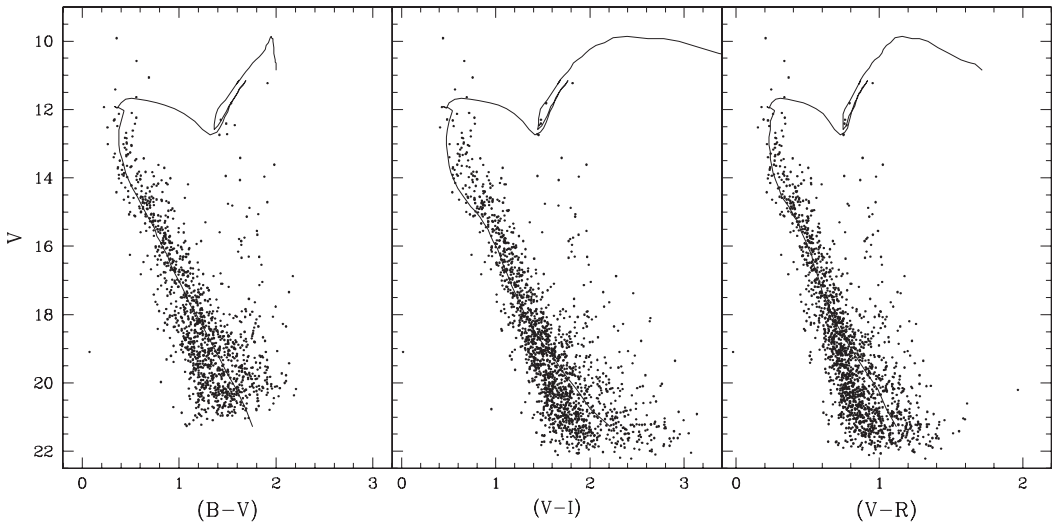

Fig. 9. CMDs for cluster NGC 1907. The isochrones by Bertelli et al. (1994) for solar metallicity and log age = 8.6 are also shown.

Table 7. Completeness factor (CF) of MS photometric data in two sub-regions.

V range	NGC 1912		NGC 1907		Field region
	$r \leq 6'$	$6' < r \leq 14'$	$r \leq 2'$	$2' < r \leq 6'$	
13–14	1.00	1.00	1.00	1.00	1.00
14–15	0.96	0.98	1.00	0.96	1.00
15–16	0.93	0.98	1.00	0.97	0.99
16–17	0.89	0.96	0.91	0.94	0.99
17–18	0.88	0.93	0.86	0.94	0.98
18–19	0.74	0.88	0.84	0.90	0.96
19–20	0.72	0.78	0.70	0.87	0.94

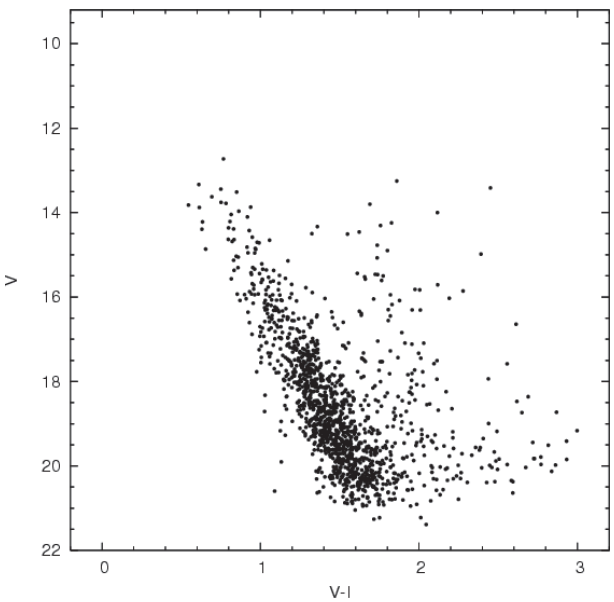

Fig. 10. V, $(V-I)$ CMD for the nearby field region.

contamination from the sample of stars in the cluster region. Proper-motion studies are ideal to decide membership, but in the absence of a proper-motion study, we used a statistical criterion to estimate the number of probable member stars in the cluster region, assuming a uniform stellar density distribution in the vicinity of the clusters. The contamination due to field stars is greatly reduced if we select a sample of stars that is located within the defined envelopes for the main-sequence (cf. Pandey et al. 2001, 2005). The same envelopes were used for the V, $(V-I)$ CMD of the field region to estimate the contamination in the cluster region due to field stars. After normalizing the area we can find the number of field stars present per unit area in each magnitude bin. The number of probable cluster members in the two subregions of the cluster was obtained by subtracting the contribution of field stars (corrected for data incompleteness) from each magnitude bin of the contaminated sample of MS stars (also corrected for data incompleteness).

The MF is often expressed by a power law, $N(\log m) \propto m^{\Gamma}$, and the slope of the MF is given as

$$\Gamma = d \log N(\log\, m)/d \log\, m, \tag{6}$$

where $N(\log m)$ is the number of stars per unit logarithmic mass interval. The classical value derived by Salpeter (1955) for the slope of IMF is $\Gamma = -1.35$. The LFs of the two subregions of the clusters NGC 1912 and NGC 1907 have been converted to the MFs using a theoretical model of Bertelli et al.

Table 8. Mass function of clusters NGC 1912 and NGC 1907.*

Cluster	Range V(mag)	Mass ($M_\odot$)	Mean log $M_\odot$	Inner region N	Inner region log ϕ	Outer region N	Outer region log ϕ	Whole region N	Whole region log ϕ
NGC 1912	11–12	3.06–2.62	0.453	7	2.016	14.0	2.317	21.0	2.493
	12–13	2.62–2.06	0.369	32.3	2.490	35.9	2.536	68.2	2.815
	13–14	2.06–1.64	0.267	25.0	2.402	48.6	2.691	73.6	2.871
	14–15	1.64–1.36	0.176	19.7	2.384	43.3	2.726	63.0	2.889
	15–16	1.36–1.14	0.097	21.9	2.456	36.2	2.674	58.1	2.880
	16–17	1.14–0.98	0.025	42.3	2.809	47.7	2.861	90.0	3.137
NGC 1907	11–12	3.70–3.17	0.537	1.0	1.173	2.0	1.474	3.0	1.884
	12–13	3.17–2.77	0.473	8.0	2.136	4.4	1.876	12.4	2.326
	13–14	2.77–2.22	0.398	9.2	1.981	21.9	2.358	31.1	2.510
	14–15	2.22–1.75	0.299	17.3	2.224	30.9	2.476	48.2	2.668
	15–16	1.75–1.43	0.201	13.6	2.191	31.9	2.560	45.5	2.715
	16–17	1.43–1.19	0.117	15.4	2.284	33.5	2.623	48.9	2.787

* The number of probable cluster members (N) were obtained after subtracting the expected contribution of field stars in each magnitude range. log ϕ represents log $(N/d\log m)$.

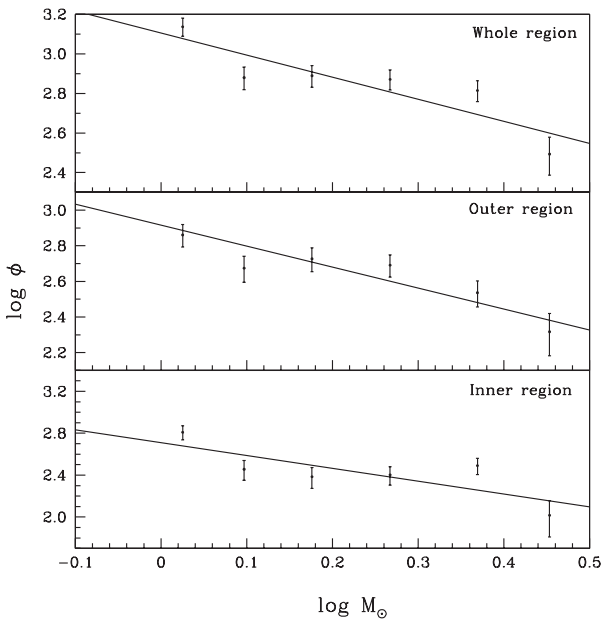

Fig. 11. Plot of the mass function for the cluster region and for the two subregions of the cluster NGC 1912. The error bars represent $1/\sqrt{N}$ errors. Continuous curves show a least-squares fit for the mass range $1.0 < M_\odot < 3.1$.

(1994); the resultant MF data are given in table 8.

Figure 11 shows a plot of $\log N(\log m)$ vs. $\log m$ for the inner region ($r \leq 6'$), outer region ($6' < r \leq 14'$), and also for the whole cluster region of NGC 1912, i.e., $r \leq 14'$. In the mass range $1.0 \leq M_\odot < 3.1$ the MF for the whole cluster region can be represented by a power law with a slope $\Gamma = -1.12 \pm 0.30$, which 'within error' is in agreement with the Salpeter value. For the above mass range the slope of the MF obtained in the inner and outer region is also given in table 9.

The mass function in the case of NGC 1907 for the inner region ($r \leq 2'$), outer region ($2' < r \leq 6'$) and for the whole cluster region ($r \leq 6'$) is plotted in figure 12. In the mass

Table 9. Mass function slopes in various regions.

Region	Mass range $M_\odot$	$\Gamma \pm \sigma$
NGC 1912		
Inner	1.0–3.1	-1.23 ± 0.48
Outer	1.0–3.1	-1.05 ± 0.24
Whole	1.0–3.1	-1.12 ± 0.30
NGC 1907		
Inner	1.2–3.2	-0.57 ± 0.32
Outer	1.2–3.2	-1.84 ± 0.56
Whole	1.2–3.2	-1.23 ± 0.21

range $1.2 \leq M_\odot \leq 3.2$ the MF for the whole cluster region ($r \leq 6'$) can be represented by $\Gamma = -1.23 \pm 0.21$, which is also in agreement with the Salpeter value. The mass functions in the inner and outer regions of the cluster (given in table 9) indicate mass segregation in the cluster region in the sense that massive stars are preferentially located in the central region of the cluster.

7. Mass Segregation

There is evidence for mass segregation in many galactic star clusters as well as in the LMC clusters, with the highest mass stars preferentially found towards the center of the cluster (see e.g., Pandey et al. 1992, 2001, 2005; Fisher et al. 1998 and references therein). To characterize the degree of mass segregation in NGC 1912 and NGC 1907, we subdivided the sample into two mass groups, ($0.74 \leq M_\odot < 1.36, 1.36 \leq M_\odot < 3.1$) and ($0.72 \leq M_\odot < 1.40, 1.40 \leq M_\odot < 3.60$), respectively. Figures 13 and 14 show the cumulative distribution as a function of the radius in two different mass groups. The figures clearly indicate an effect of mass segregation in the cumulative distribution in the sense that most massive stars tend to lie near the cluster center. The

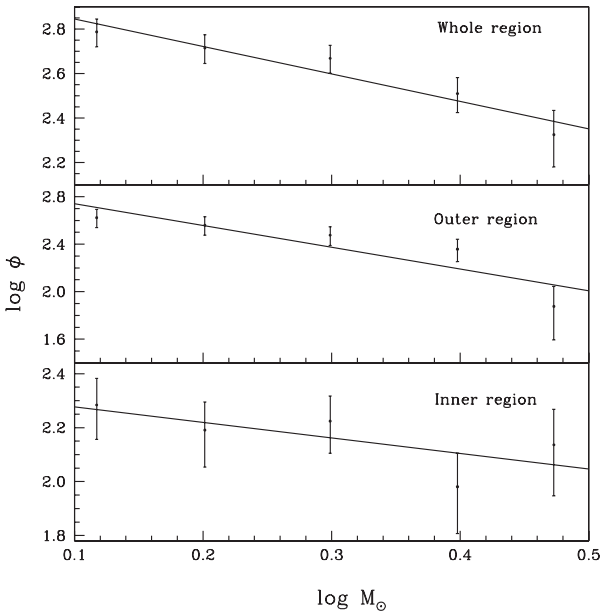

Fig. 12. Same as figure 11, but for NGC 1907.

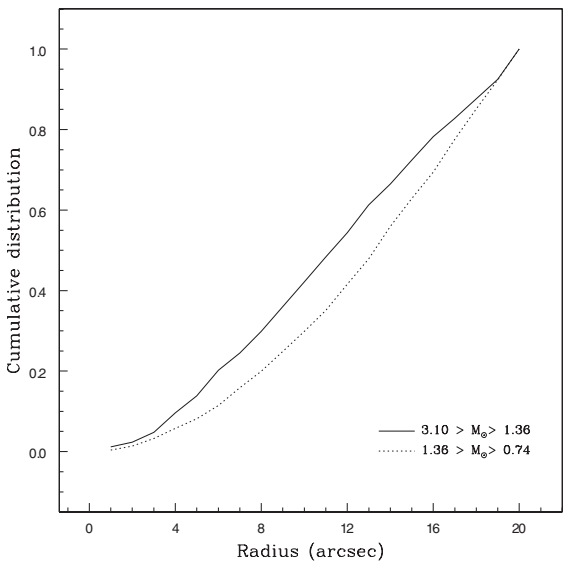

Fig. 13. Cumulative radial distribution in NGC 1912 for different mass intervals.

Kolmogorov–Smirnov test confirms the statement that the cumulative distribution of most massive stars in the clusters is different at a confidence level better than 99% from the cumulative distribution of relatively less massive stars.

We have to estimate the relaxation time to decide whether the mass segregation discussed above is primordial or due to dynamical relaxation. Because of dynamical relaxation, low-mass stars in a cluster may possess the largest random velocities; consequently, these will try to occupy a larger volume than high-mass stars (cf. Mathieu 1985; Mathieu & Latham 1986; McNamara & Sekiguchi 1986). For determining the dynamical relaxation time, $T_{\rm E}$, we used the relation

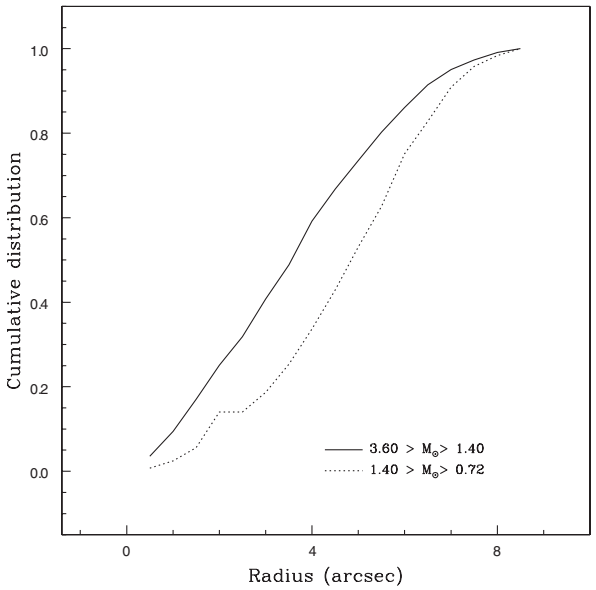

Fig. 14. Same as figure 13, but for NGC 1907.

Table 10. Dynamical relaxation time, $T_{\rm E}$, and parameters.*

Parameter	NGC 1912	NGC 1907
N	600	400
$R_{\rm h}$	2.85 pc	1.55 pc
$\bar{m}$	1.33 $M_\odot$	1.38 $M_\odot$
$T_{\rm E}$	40 Myr	14 Myr
Age	300 Myr	300 Myr

* Parameters are used to estimate $T_{\rm E}$ for the clusters NGC 1912 and NGC 1907.

$$T_{\rm E} = \frac{8.9\times10^5 N^{1/2} R_{\rm h}^{3/2}}{\bar{m}^{1/2}\log(0.4N)}, \quad (7)$$

where N is the number of cluster stars, $R_{\rm h}$ the radius containing half of the cluster mass and $\bar{m}$ the average mass of cluster stars (Spitzer & Hart 1971). The total number of MS stars and the total mass of the MS stars in the given mass range ($0.74 \leq M_\odot \leq 3.1$ for NGC 1912; $0.72 \leq M_\odot \leq 3.6$ for NGC 1907) were obtained with the help of the LF. This mass should be considered as a lower limit to the total mass of the clusters. For the half mass radius, we used half of the cluster extent. Various parameters used to estimate the dynamical relaxation time $T_{\rm E}$ for the clusters are given in table 10. Using these numbers, the estimated relaxation time, $T_{\rm E}$ comes out to be significantly smaller than the age of the clusters. This indicates that dynamical relaxation may be one of the reasons for the observed mass segregation in these clusters.

8. Synthetic CMDs

During the last decade, synthetic CMDs have been used to study various properties of clusters, e.g., the MF and the influence of unresolved photometric binaries on the LF, etc. (cf. Sandhu et al. 2003 and references therein). By comparing the synthetic integrated luminosity function (ILF)

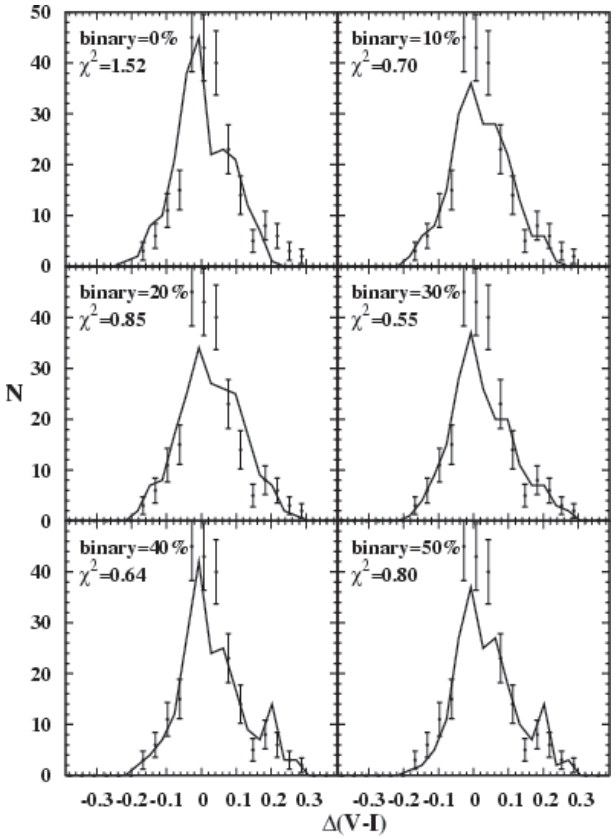

Fig. 15. Observed (filled points with error bars) and synthetic $\Delta(V-I)$ distribution (continuous curve) for NGC 1912.

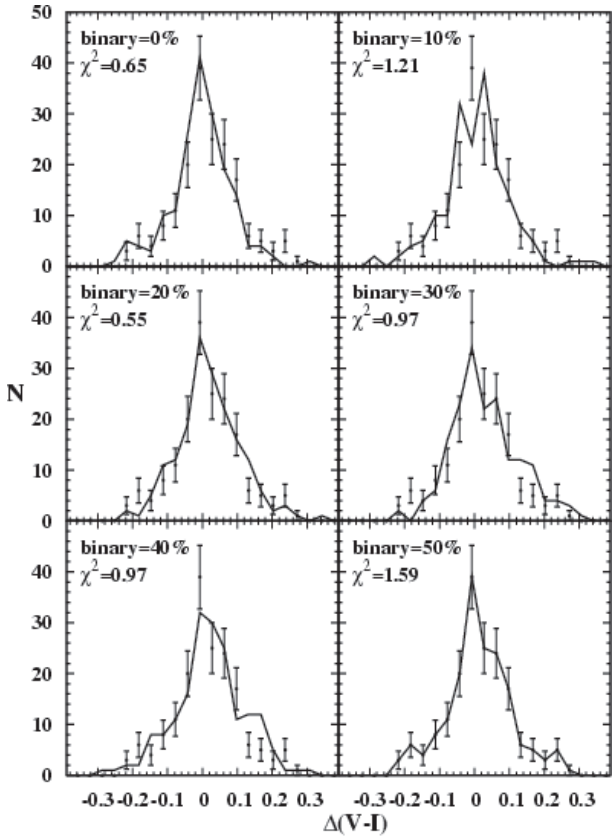

Fig. 16. Same as figure 15, but for NGC 1907

and the synthetic colour distribution with the corresponding observed distribution, they estimated the photometric binary content in three intermediate-age open clusters. Following the procedure of Sandhu et al. (2003), we calculated $\Delta(V-I) = (V-I)_* - (V-I)_{\rm MS}$ for each star, where $(V-I)_*$ is the observed colour of a star and $(V-I)_{\rm MS}$ is the corresponding colour of the MS. The $\Delta(V-I)$ frequency distribution of stars brighter than $V \sim 15$ mag (NGC 1912) and $V \sim 17$ mag (NGC 1907) of the statistically cleaned CMD was compared with the $\Delta(V-I)$ frequency distribution of the synthetic CMDs (for details see Sandhu et al. 2003). The statistically cleaned CMDs were obtained using the following statistical procedure. For a randomly selected star in the $V,(V-I)$ CMD of the field region, the nearest star in the cluster's $V,(V-I)$ CMD within $V \pm 0.25$ and $(V-I) \pm 0.125$ of the field star was removed. While removing the stars from the cluster CMD, the number of stars in each luminosity bin was maintained as per the completeness corrected LF (cf. section 6). A comparison of the observed and synthetic distributions along with the χ^2 values is shown in figures 15 and 16 for NGC 1912 and NGC 1907, respectively, which indicates a photometric binary content of 30±10% and 20±10% for clusters NGC 1912 and NGC 1907, respectively.

9. Discussion and Conclusion

CCD photometric observations in a wide field around open clusters NGC 1912 and NGC 1907 were carried out for the first time. The data form a base for studying the spatial structure and the MF. Field-star contamination was also estimated from a nearby region. The data completeness was determined empirically as a function of the brightness and stellar crowding. The cluster parameters were determined by fitting the convective core overshoot isochrones given by Bertelli et al. (1994) to the V, $(B-V)$, and V, $(V-I)$ colour–magnitude diagrams of the cluster. The main conclusions of the present work are given in table 11.

Table 11. Parameters of the clusters.

Parameter	NGC 1912	NGC 1907
Distance (pc)	1400 ± 100	1760 ± 100
$E(B-V)$ (mag)	0.25 ± 0.05	0.38 ± 0.05
Log age	8.5 ± 0.1	8.6 ± 0.1
Total mass ($M_\odot$)	$\sim 800^*$	$\sim 550^\dagger$
Number of stars	$\sim 600^*$	$\sim 400^\dagger$
Average mass ($\bar{m}$)	$\sim 1.33^*$	~ 1.38
Linear diameter (pc)	~ 5.7	~ 3.1

* Mass range ($0.7 < M_\odot < 3.1$).
† Mass range ($0.7 < M_\odot < 3.6$).

The distance, linear radius, number of stars, and total mass of the cluster are important parameters to model the cluster

evolution; e.g., by using N-body simulations of NGC 1912 and NGC 1907, de Oliveira et al. (2002) concluded that these two clusters were born in different regions of the Galaxy, and ruled out the candidature of these clusters for a physical pair. However, they mentioned that it would be necessary to analyze deep wide field CCD photometry for a more conclusive result about the apparent absence of a tidal link between clusters NGC 1907 and NGC 1912. The present study was an effort to provide a deep and wide photometry of clusters NGC 1912 and NGC 1907. The main conclusions of the present work are:

1. The distances to clusters NGC 1912 and NGC 1907 are found to be 1400 ± 100 pc and 1760 ± 100 pc, respectively. The significant difference in the distances of the clusters supports the conclusion of de Oliviera et al. (2002) that they were formed in different parts of the Galaxy.
2. The extent of the cluster NGC 1912 is about $\sim 14'$ whereas the core of the cluster is found to be varying significantly with the limiting magnitude. In the case of NGC 1907, the core radius and the cluster extent are estimated to be $2'$ and $6'$, respectively.
3. The MF of the inner region, outer region as well as for the whole cluster is quite noisy for both clusters. However, for the whole cluster region the slope of the MF, within errors, is equal to the Salpeter value.
4. Both of the clusters are dynamically relaxed, since the relaxation time is much shorter than the age of the clusters. The observed mass segregation in the clusters can therefore be a result of the dynamical evolution of the system.
5. A comparison of the observed CMDs of the clusters with synthetic CMDs gives a photometric binary content, in the mass ranges $1.0 \leq M_{\odot} \leq 3.1$ and $1.2 \leq M_{\odot} \leq 3.2$ as $30 \pm 10\%$ and $20 \pm 10\%$ for the cluster NGC 1912 and NGC 1907, respectively.

The authors are thankful to an anonymous referee for useful comments that improved the presentation of the paper. AKP is thankful to the DST (India) and JSPS (Japan) for providing funds to visit Kiso Observatory to carry out observations and to the staff of Kiso Observatory for their generous help during the stay. He also thanks to the National Central University, Taiwan for the financial support during his visit to NCU.

References

Becker, W. 1963, Z. Astrophys., 57, 117
Bertelli, G., Bressan, A., Chiosi, C., Fagotto, F., & Nasi, E. 1994, A&AS, 106, 275
Collinder, P. 1931, Ann. Lund Obs., 2
de Oliveira, M. R., Fausti, A., Bica, E., & Dottori, H. 2002, A&A, 390, 103
Fisher, P., Pryor, C., Murray, S., Mateo, M., & Richtler, T. 1998, AJ, 115, 604
Hoag, A. A. 1966, Vistas Astron. 8, 139
Hoag, A. A., & Applequist, L. 1965, ApJS, 12, 215
Hoag, A. A., Johnson, H. L., Iriarte, B., Mitchell, R. I., Hallam, K. L., & Sharpless, S. 1961, Publ. US Naval Obs., 17, 347
Jacobson, H. R., Cummings, J., Deliyannis, C. P., Steinhauer, A., & Sarajedini, A. 2002, BAAS, 34, 1308
Johnson, H. L. 1961, Lowell Obs. Bull., 5, N8
Kaluzny, J., & Udalski, A. 1992, Acta Astron., 42, 29
Kharchenko, N. V., Piskunov, A. E., Röser, S., Schilbach, E., & Scholz, R. D. 2005, A&A, 438, 1163
Kholopov, P. N. 1969, SvA-AJ 12, 625
King, I. R. 1962, AJ, 67, 471
Landolt, A. U. 1992, AJ, 104, 340
Mathieu, R. D. 1985, in Proc. IAU Symp., No. 113, 427
Mathieu, R. D., & Latham, D. W. 1986, AJ, 92, 1364
McNamara, B. J., & Sekiguchi, K. 1986, ApJ, 310, 613
Pandey, A. K., Mahra, H. S., & Sagar, R. 1992, BASI, 20, 287
Pandey, A. K., Nilakshi, Ogura K., Sagar, R., & Tarusawa, K. 2001, A&A, 374, 504
Pandey, A. K., Sharma, S., & Ogura, K. 2006, MNRAS, 373, 255
Pandey, A. K., Upadhyay, K., Ogura, K., Sagar, R., Mohan, V., Mito H., Bhatt, H. C., & Bhatt, B. C. 2005, MNRAS, 358, 1290
Purgathofer, A. 1961, Z. Astrophys., 53, 151
Purgathofer, A. 1964, Ann. Univ. Sternw. Wien, 26, no.2
Salpeter, E. E. 1955, ApJ, 121, 161
Sandhu, T. S., Pandey, A. K., & Sagar, R. 2003, A&A, 408, 515
Spitzer, L., Jr., & Hart, M. H. 1971, ApJ, 164, 399
Stetson, P. B. 1992, in ASP Conf. Ser. 25, Astrophysical Data Analysis Software and System I., ed. D. M. Warrall, C. Biemesderfer, & J. Barnes (San Francisco: ASP), 297
Subramaniam, A., & Sagar, R. 1999, AJ, 117, 937 (SS99)
Trumpler, R. J. 1930, Lick Obs. Bull., 14, 154